

CASBI: Chemical Abundance Simulation Based Inference

Giuseppe Viterbo

June 30, 2024

Contents

1 Abstract	2
2 Previous work	3
2.1 The reconstruction of the Assembly history of the Milky Way	3
3 CASBI: Chemical Abundance Simulation Based Inference	7
3.1 Simulation Based Inference	7
3.2 Simulator	9
3.3 Two step Inference	9
3.4 Realistic halo and 1 step Inference	11
3.5 Free Form Flow as a surrogate simulator	14
3.6 Calibration	14
4 Analysis	15
4.1 NIHAO UHD	15
5 Conclusion	16
5.1 Future work	16
5.1.1 semianalitic model	16
5.1.2 Number halos has a free parameter: hierarchical sbi	16
5.1.3 True test: GAIA	16

Chapter 1

Abstract

Galaxies evolve through merging events and destroy lower-mass systems over their lifetimes. The contribution that those lower-mass system brings to the modern picture has been frozen in stellar halos by the long orbital timescales, making the relicts of these objects retain part of their initial progenitor orbit. But dynamical information is not enough to disentangle these components, and the complementary chemical information helps to characterize these building blocks. In fact, merging events tend to quench the star formation rate of these objects, making the chemical abundance plane (iron abundance against α element abundance) a distinct imprint that retains information on the conditions of formation of their stars, like the total mass and the age of the system until the merging event. These theoretical background allows us to attempt to decompose the stellar halo into its components, unraveling the merging history. In the modern era of large N-body galaxy simulations, we recast this problem into an SBI pipeline to recover the properties of this building block, (e.g. total stellar mass, infall time, ...) using the chemical abundance plane as observables. We therefore present CASBI (Chemical Abundance Simulation Based Inference), a python package to recover the posterior probability of properties of building blocks of Milky Way like galaxy's halo. Moreover, CASBI incorporate conditional neural network architectures as generator to obtain observables from parameters, smoothly interpolating on region of the parameters space that weren't fully covered during the N-body simulations.

Chapter 2

Previous work

2.1 The reconstruction of the Assembly history of the Milky Way

Inferring the assembly history of the Milky Way is a challenging task, even in the era of the astrometric Gaia mission and its 6 dimensional phase space data, and the complementary chemical information obtained from the wide-field spectroscopic programs such as the GALAH survey [6], the H3 survey [3], APOGEE [17], RAVE [24], SEGUE [29], and LAMOST [4]. The dynamical times of the accreted objects are far longer than the age of the host galaxy, allowing the phase space to retain part of the information on the original orbit parameters. On the other hand, the chemical space is dependent on the star formation history, in particular type II SNe produce α -elements and iron with a almost constant ratio, while type Ia SNe produce more efficiently iron. Another factor that governs the chemical space is the total mass of the galaxy, since the more massive galaxies are more capable to resist the expulsion of metals due to feedback mechanism. The crossmatch between Gaia and spectroscopic data allowed for the discovery of the "Gaia-Sausage-Enceladus" (GSE) ([2], [11]), a massive accretion event whose remnant now dominates the observation of the inner stellar halo of our Galaxy. The GSE is described as major structure with mostly highly eccentric, retrograde orbit with a chemical abundance distribution of stars that highly distinct from the thin and thick disc star of the Milky Way, as it is possible to see in Fig 2.1.

Robustly identify distinct structure is challenging, and disentangle the components in fully phase mix situations is nearly impossible. In order to characterize the assembly history [5] propose to use the "CARDs", the chemical abundance ratio distributions of the stars, obtained from a subsample of accreted object candidate from the FIRE-2 zoom-in cosmological simulations of MW-mass galaxies [28]. Although similar to CASBI on how to leverage N -body simulations, this method do not recovers posteriors for the parameters of the accreted objects but rather considers the host halo as a linear combinations of templates CARDS

$$\text{CARD}_{\text{halo, model}}(x_d) = \sum_i \sum_j A_{ij} \text{CARD}_{\text{temp},ij}(x_d | M_{\text{sat},i}, t_{100,j}), \quad (2.1)$$

treating each coefficient A_{ij} as the fraction of mass contribution from the accretion event of the template satellite with mass $M_{\text{sat},i}$ and quenching time $t_{100,j}$, and tries to recover those coefficients by maximize a loss that compares the observed CARDs with the combination of the templates. An example of template constructed from dwarf galaxies is presented in Fig. 2.2. The template

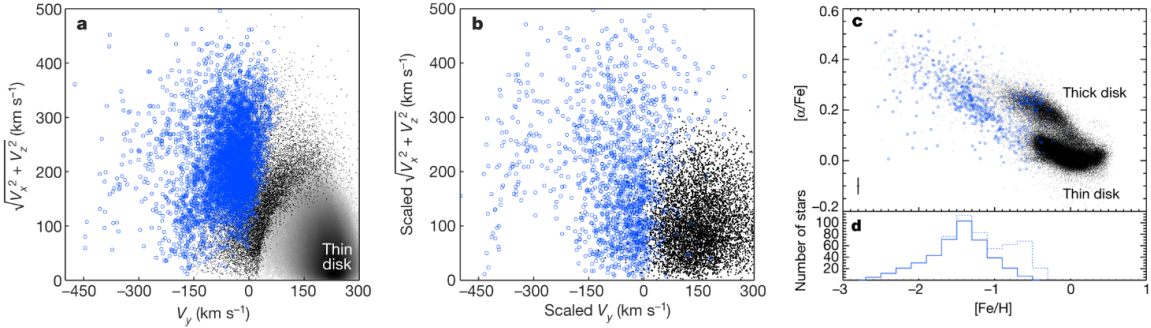


Figure 2.1: Left panel: Toomre diagram for Gaia DR2 data where in blue are stars selected to pick out the GSE structure. Middle panel: similar to the left panel but with simulated data of a minor merger, resulting in a less concentrated structure, mostly due to the fact that a more massive structure is more able to retain its original orbital properties. Right panel: the star in blue are the same of the left panel crossmatched with the APOGEE chemical information. [The figure is from [11]].

that were used belong to the catalog of star particles in the FIRE simulations belonging to dwarf galaxies, stellar streams and phase-mixed debris constructed in [19]. This method and CASBI share two more aspect: 1. Both of these methods are meant to be used on simulations, and the integrations of observational data is not yet implemented, even though theoretically possible. 2. Both rely on the assumption that the chemical space of accreted and isolated dwarf galaxies is very similar, due to ram pressure quenching the star formation history of the accreted object and hence 'freezing' these abundance ratios at the infall time.

Another approach is presented in [8], which takes advantage of the mass-metallicity relation to decompose the metallicity distribution functions (MDF) of the host galaxy as a mixture of accreted halo's MDF, assumed gaussian for each of these building blocks. This decomposition rely on [14] that demonstrated that at the dwarf mass scale, not only the average metallicity vary with the mass, but the width of the MDF also varies, with the lowest mass dwarf having a wider spread of metallicities. The Likelihood that is used in this work for the $[\text{Fe}/\text{H}]$ distribution, indicated as \mathbf{z} is then:

$$P(z|N, L_i, \mu_i, \sigma_i) = \frac{1}{\sum L_i} \sum_{i=1}^N L_i \mathcal{N}(z|\mu_i, \sigma_i), \quad (2.2)$$

where they have assumed that the number of stars in the sample scales linearly with galaxy luminosity L_i , that the μ_i follows a mass-metallicity relation and that the σ_i depend on the galaxy luminosity as described in [14]. Similarly to CASBI, this method has the problem of having a variable number of parameters, making it difficult to sample in practice, so to tackle this problem they decided to bin the luminosities L_j and count the number of contribution from each bin N_j . In order to perform the inference, they adopted a nested sampling scheme to obtain a posterior distribution for the number of galaxies in each luminosity bin, which can be considered a proxy for the star mass. The posterior probability for the Milky Way halo is reported in Fig. 2.3. The samples used in this posterior were obtained from different spectroscopic surveys after applying various cut to avoid contamination from thick disc stars. The cut were made based on parallax distance, radial distance, height with respect to the plane of the galaxy, and only stars with a retrograde orbit $v_\phi < 50$ were selected.

In CASBI we adopt the same superimposition of the components contribution, but we do not

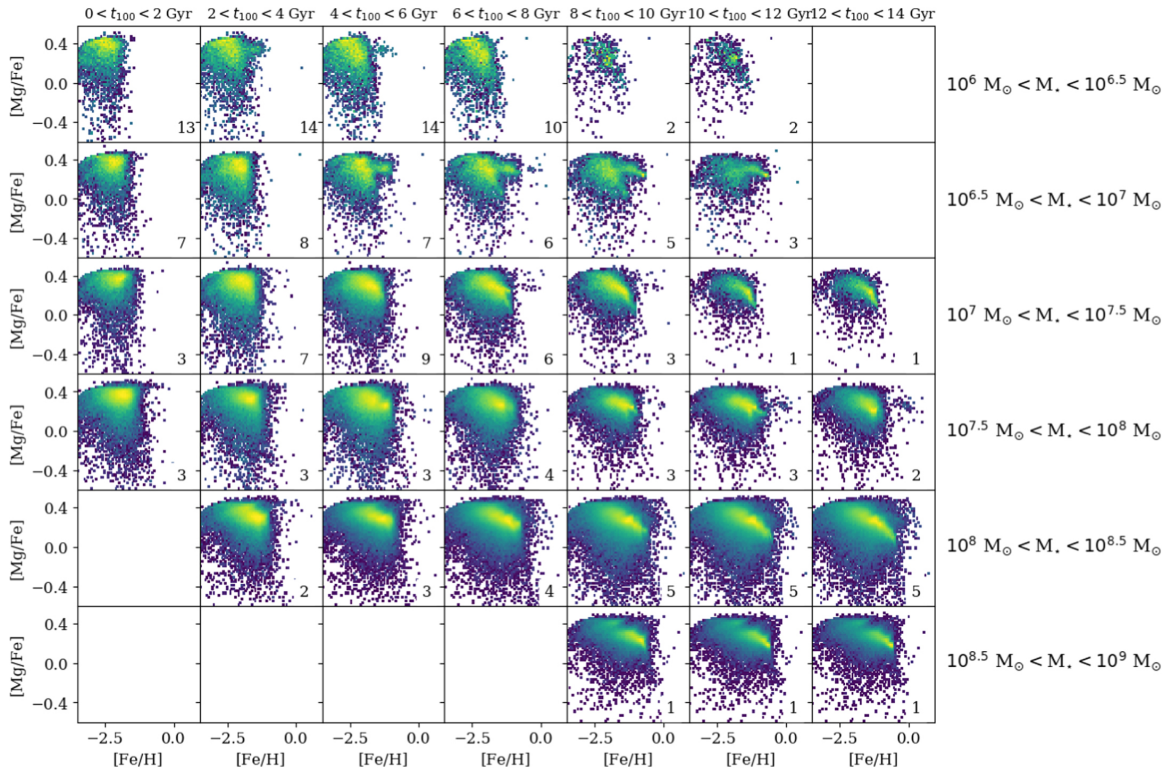


Figure 2.2: Template for accretion events constructed using dwarf galaxy in [5]. More massive dwarf galaxies have CARDs that extend to higher metallicities. At fixed stellar mass, galaxies that assemble more quickly (lower t_{100}) have more density at higher $[\text{Mg}/\text{Fe}]$ than the component with a more extended star formation history.

assume neither a prefix or an analytical form for the joint distribution of the chemical abundances, relaxing these assumption and relying only on the available samples from the N-body simulations. Also a possible limitation of our method is that we do not take into consideration a distinction between destroyed and surviving accreted dwarf galaxy. This can lead, as described in [18] to a -0.3 dex offset of the mass metallicity [14] relation that might be necessary to take into account.

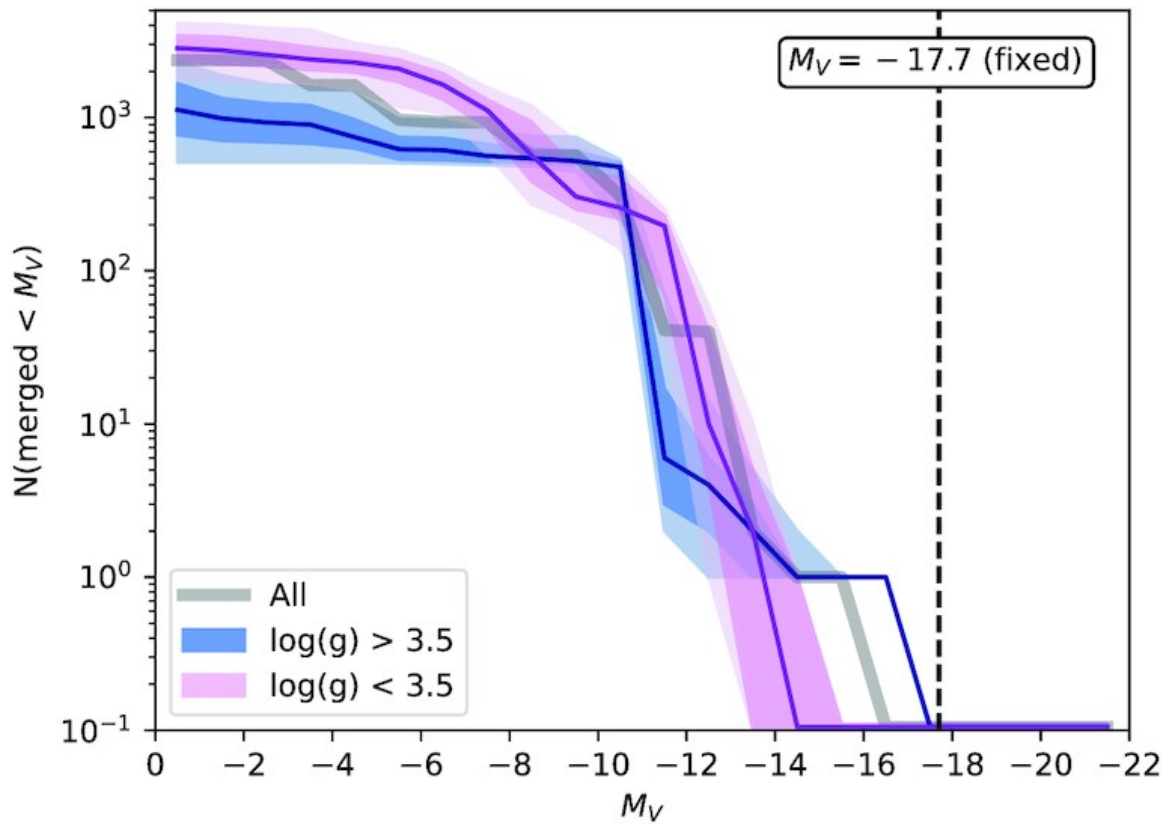


Figure 2.3: The estimated number of destroyed dwarf galaxy in the MW halo. The separation in two bin value of $\log(g)$ because dwarf stars and giants can have different metallicity biases.

Chapter 3

CASBI: Chemical Abundance Simulation Based Inference

3.1 Simulation Based Inference

CASBI is a Simulation Based Inference (SBI) package to recover the properties of building blocks of Milky Way like galaxy's halo from observations of the chemical abundance plane. The SBI framework has existed along side the more traditional likelihood based inference methods for quite some years already, having its root in the Approximate Bayes Computation [23], and it has been used in a variety of fields, from cosmology to particle physics. The main difference between SBI and likelihood based methods, like MCMC, is that the former do not require the likelihood function to be known, but rather rely on a simulator to generate synthetic data \mathbf{x} once the input parameters θ are passed to it, and the inference pipeline is trained based on data-parameters pairs (\mathbf{x}, θ) .

Recent advance of this technique was made possible by the use of machine learning models to emulate conditional probability distributions, a technique know as Neural Density Estimation (NDE) [20]. The NDE is achieved by training a Normalizing Flow architecture, a generative model that allows to obtain samples from a complex distribution $p(x)$ by constructing a series of **bijection** transformations $f_{\phi_i}^i$ that map x to a latent space z that is distributed as a simple distribution, like a Gaussian. Accordingly to [13], implementing the transformations as Neural Network with parameters ϕ_i , in the end the models learns the following schema:

$$p(x) \sim x \equiv h_0 \xleftarrow{f_{\phi_1}^1} h_1 \xleftarrow{f_{\phi_2}^2} h_2 \dots \xleftarrow{f_{\phi_K}^K} h_K \equiv z \sim \mathcal{N}(z; 0, \mathcal{I}), \quad (3.1)$$

by maximizing the negative log likelihood as loss function and using the change of variable formula as follows:

$$\begin{aligned} \log p(x) &= \log p(z) + \log \left| \det \left(\frac{\partial z}{\partial x} \right) \right| \\ &= \log p(z) + \sum_{i=1}^K \log \left| \det \left(\frac{\partial h_i}{\partial h_{i-1}} \right) \right| \\ &= \log p(z) + \sum_{i=1}^K \log \left| \det \left(\frac{\partial f_{\phi_i}^i(h_{i-1})}{\partial h_{i-1}} \right) \right|, \end{aligned} \quad (3.2)$$

where the last term is the sum of the log determinant of the Jacobian of the transformations $f_{\phi_i}^i$. Once the model is trained it is easy to sample from the distribution $p(x)$ by sampling from the latent space z and applying the inverse transformations $(f_{\phi_1}^1)^{-1} \circ \dots \circ (f_{\phi_K}^K)^{-1}$. In order to keep the sum of log determinant tractable, the use of *Coupling layers* allows to split the input x along its dimensions and apply a transformation only to a subset of the dimensions, using the other as input for the transformation and keeping it fixed. The subset is then changed at each layers, allowing to have a permutation invariant transformation. The transformations $f_{\phi_i}^i$ are usually very simple invertible transformation like a translation and a scaling, or splines functions. The choice of the invertible function can affect the expressivity of the model, defined as the capability of approximate more complex multivariate distribution, at the cost of more parameters, computational time and inference time.

Following the discussion presented in [12], in Bayesian analysis we have the choice to approximate either the Posterior, the Likelihood or the Likelihood ratio, and this choice depend mostly on the problem that one wants to solve.

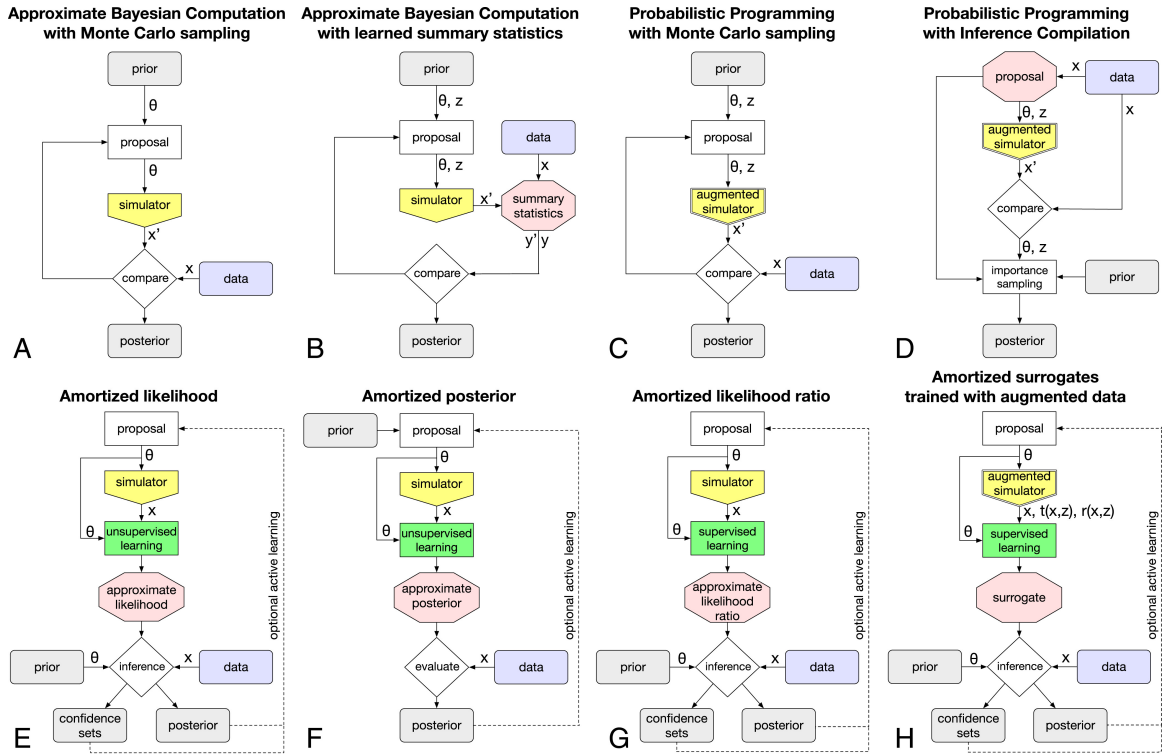


Figure 3.1: Different approaches to Simulation Based Inference, from [1].

In our case, due to the complexity of the Likelihood distribution of the chemical abundance space, we choose to approximate the Posterior distributions, and so we adopted the Neural Posterior Estimate (method F in Figure 3.1) that can be trained using the negative loglikelihood as loss function:

$$\begin{aligned}\mathcal{L}_{NPE}(\theta) &= -\mathbb{E}_{\mathcal{D}_{train}} \log \hat{\mathcal{P}}(\theta_i | x_i) \\ &= -\mathbb{E}_{\mathcal{D}_{train}} \log \left(\frac{p(\theta)}{\tilde{p}(\theta)} q_\omega(\theta_i, x_i) \right),\end{aligned}\tag{3.3}$$

where our Posterior distribution $\hat{P}(\theta_i|x_i)$ is approximated by the product of the ratio of the prior $p(\theta)$ and proposal distribution $\tilde{p}(\theta)$ and the neural conditional distribution $q_\omega(\theta_i, x_i)$, parametrized by the parameters ω .

Many excellent framework for handling SBI analysis are already available, and CASBI is build on top of the `ltru-ili` python package [12]. In particular, CASBI analysis were performed relying on the `sbi` backend [25] to train a *Neural Posterior Estimate*¹ of the parameters' posteriors. The preprocessing of the data is described in Section 3.2, the details of the training of the NPE is described in Section 3.3.

3.2 Simulator

The data-parameters pairs $(\mathbf{x}, \boldsymbol{\theta})$ needed to train the NPE are obtained from the Numerical Investigation of a Hundred Astrophysical Objects (**NIHAO**) project [27]. The **NIHAO** is a set of 100 cosmological zoom-in hydrodynamical simulations with halos that range from dwarf ($M_{star} \sim 5 \times 10^9 M_\odot$) to Milky Way like ($M_{star} \sim 2 \times 10^{12} M_\odot$). In order to handle these simulations, in CASBI the preprocessing is done with the use of the functions available in `pynbody` [22]. In Fig. 3.2 we show face on samples of galaxies in the **NIHAO** simulations set.

Similarly to [5] and [8], we rely on the assumption that once the accreted object falls into the gravitational potential of the Milky Way like galaxy its star formation rate is halted, so we can treat each of the snapshot in this simulations as a possible building block of galactic halo.

The construction of the observables is done in by aggregating multiple subhalo into a single stellar halo. In order to create subhalo we construct 2D histogram, referred to as \mathbf{x}^i , by binning the chemical abundance plane $[[O/Fe], [Fe/H]]^2$ for each of the snapshot available in **NIHAO**. We have also filter the galaxies to have object with a total stellar mass lower than the stellar mass of the Large Magellanic Cloud ($M_{star} < 6 \times 10^9 M_\odot$), the largest accreted object by the Milky Way. The 2D histogram have 64×64 pixels, and minimum and maximum values set after filtering all the stars that were outside the 0.01 percentile in either metallicity or α element abundance. Each of the x_i is uniquely identifiable trough the `Galaxy_name` attribute. The set of all possible subhalos is defined as 'Template Library'. The actual stellar halo observable $\mathbf{x}^j = \sum_i^{N_{sub}^j} x_i^j$ used in CASBI is then a super imposition of N_{sub} of these 2D histograms, where the N_{sub}^j is the number of accreted objects present in the j -th galaxy halo. The actual choice of how to sample from the template library created from the **NIHAO** simulations can be adapted, we tested to randomly sample in 3.3 and to use a more physically informed approach by using a luminosity function and a total stellar mass budget in Section 3.4.

The goal of CASBI is to beeing able to recover θ^i for each of the subhalos in the galactic halo from the observable $\mathbf{x}^j = \sum_i x_i^j$, and gaining insight on how many subhalos there are. Among all the possible parameters available from the simulations, we have decided to limit ourself to stellar mass M_{star} and age of the galaxy τ , also called infall time due to their equivalence in the assumption of quenched star formation after accretion.

3.3 Two step Inference

The objective of the inference is not trivial, since in order to recover the parameters of the building blocks of the Milky Way like galaxy we need to fix the dimensionality of the priors. This is equivalent

¹The `sbi` backed implement NPE using `nflows` [10]

²They are respectively proxy for α elements abundance and metallicity

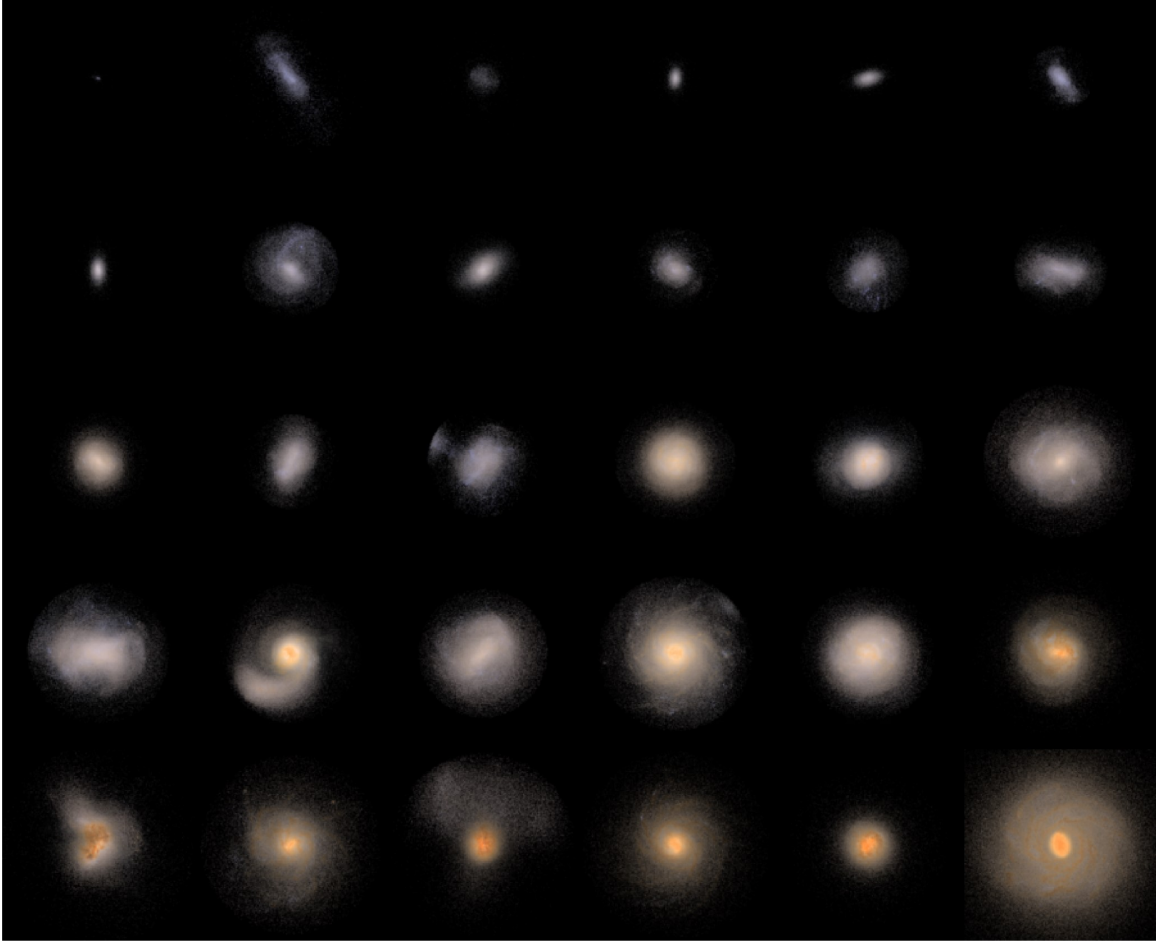


Figure 3.2: Face on **NIHAO** galaxies from [27].

to have complete knowledge on the number of substructure that are present in the galactic halo. In the case of not fully phase mixed structure, the dynamical information could be used to help to disentangle this structure, and also to separate them from the host halo background. In CASBI we do not leverage on this information because it would require to construct stellar halo that have aggregated objects that are not dynamically biased. We leave this integration for future work. We decided to tackle this problem in the case of fully mixed remnants separating the inference in two steps, in the first we infer the number of subhalos and in the second the parameters of each of the subhalos:

1. **Inference of the number of substructure:** In this step we train a NPE to recover the posterior distribution of the number of substructure N_{sub} , by using the observable \mathbf{x}^j . The prior for the parameter is assumed to be uniform between 2 and 100. This boundaries were selected in accordance to the order of magnitude of substructures found in [8]. For each of the possible N_{sub} we extract 1000 $x^j = \sum_{i=1}^{N_{sub}} x_i^j$ from the **NIHAO** simulations, in order to have a total of almost 10^5 SBI training couples (N_{sub}^j, x^j), with 20 % used as validation, and

we use the same process to generate almost 10^4 test set samples, making sure that the same combinations of `Galaxy_name` attribute weren't shown in training and test. The training of the NPE is done using the `sbi` backend, using 4 `nsf` (neural spline flow) with 10 layers and 100 neurons each. In order to take full advantage of the image-like structure of the data, we adopt as embedding network a Convolutional Neural Network (CNN) to reduce the dimensionality of the input of the NPE from 64×64 to 128. The CNN had 3 convolutional layers with 8, 16 and 32 filter, 3 maxpooling layers and 3 fully connected layers with 512, 256, 128 neurons. In this step we have not impose that the N_{sub} must be a discrete variable, and we have decided to just truncate the inferred value to the closest value. To the knowledge of the author no SBI framework has implemented a way of dealing with the inference of discrete random variables, so we leave a more precise implementation as a future work. We propose instead another method to obtain the number of substructure, by casting this inference as a classification problem. We use a SkipConnection CNN³, considering the number of substructure as the label to assign to each x^j .

2. **Inference of θ^j :** Once we have the estimate \tilde{N}_{sub} , whether using dynamical information, the inference pipeline or the classification method, we can proceed to the inference of the parameters θ_1^j . The prior for the parameters are assumed to be uniform between the minimum and maximum values available for the galaxies that we have filtered from the **NIHAO** simulations. We extract 10^5 random samples of \tilde{N}_{sub} snapshots from the **NIHAO** simulations, and we construct the observable couples $(x^j, (\theta_1^j, \dots, \theta_{\tilde{N}_{sub}}^j))$, with 20 % used as validation. We repeat the same process to generate 10^3 test set samples, making sure that the same combinations of `Galaxy_name` attribute weren't shown in training and test to perform calibration of the inference model. The training of the NPE is done using the `sbi` backend, using 4 `nsf` (neural spline flow) with 10 layers and 100 neurons each. Once again we use the same CNN architecture of the previous step as embedding for our observation x^j .

Even though highly modular, this two step inference has some limitations: the accuracy and calibration of the second step are heavily depend on the ability of the first step to recover the number of sunhalos and hence to constrain the dimensionality of the prior for the second step. We expected the pipeline to be able to recover most of the information from the most massive subhalos, due to the degeneracy in the abundance plane of the less massive and components and the more distinct feature of the more massive one. The second problem is linked to the linear scaling of the parameter dimension as a function of the number of subhalos. In a realistic case we expect to have order of ≈ 100 subhalos, resulting in a parameter space of dimensionality $2^*100 = 200$. In order to reduce the impact of these two problems we rethink the inference pipeline, presented in the next section.

3.4 Realistic halo and 1 step Inference

In order to avoid the need for a two step inference and still retaining the possibility to access to the information on how many subhalos populate a given abundance plane, we have decided to condition the SBI model to retrieve the i -most massive subhalo of the j -th stellar halo. In this way the NPE is trained on $(x, \theta) = (i, x^j, \theta_i^j)$ pairs, where $x^j = \sum_i x_i^j$ and the x_i^j are ordered accordingly to their stellar mass. In this way the j -th stellar halo abundance plane is shown as many times as the number of subhalos present in it, so in order to guide the model into inferring the right parameters θ_i^j the

³The architecture is the same as the embedding network described before with the addition of the Skip Connection layer in the fully connected layer, where the output of the previous layer gets added to the output before being passed through the activation function, alleviating the vanishing gradient problem and allowing for better accuracy.

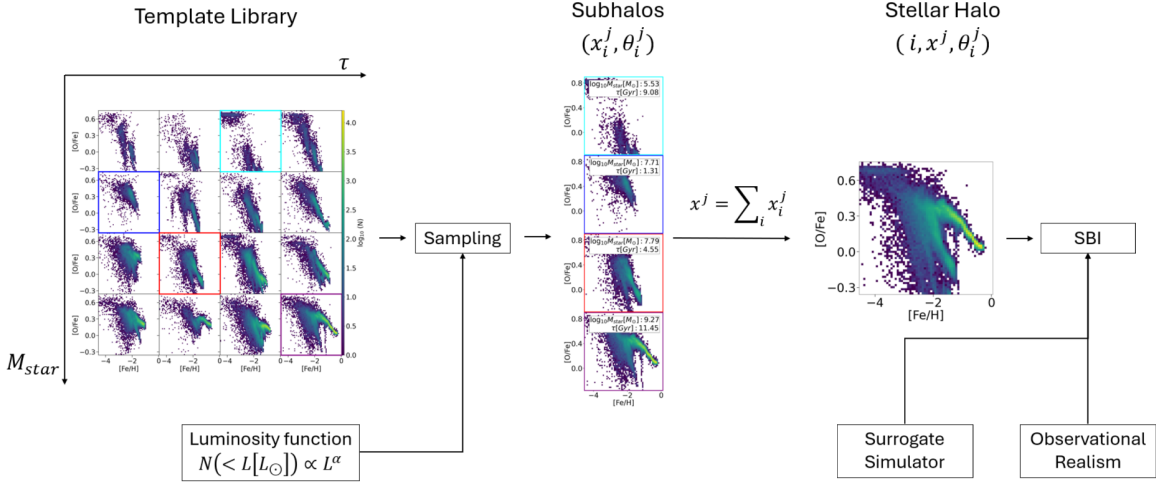


Figure 3.3: CASBI pipeline.

embedding is conditioned on the integer i -th by concatenating it to each input of the fully connected layers of the CNN used to embed the observations, and it is concatenated also before passing the embedded information to the Normalizing Flow.

In order to be more realistic in the creation of a mock galaxy halo we have decided to adopt a sampling scheme for the subhalos that is based on the luminosity function described in [15]. The luminosity function described the subhalo distribution in a range of luminosities that spans from $M_V = -2$ all the way to the luminosity of the Large Magellanic cloud:

$$\frac{dN}{dM_V} = 10 \times 10^{0.1(M_V+5)} \quad (3.4)$$

we can then manipulate this equation to express it as a function of the Luminosity in solar luminosity L :

$$\begin{aligned} \frac{dN}{dL} &= \frac{dN}{dM_V} \times \frac{dM_V}{dL} \\ &= 10^{0.1(M_{V,\odot} - 2.5\log_{10}(L) + 5) + 1} \times (-2.5L^{-1}) \sim L^{-1.25} \end{aligned} \quad (3.5)$$

which in the end can be integrated to obtain the number of subhalos with luminosity lower than L that we are going to adopt for sampling stellar halo:

$$N(< L) = K \times L^\alpha, \quad (3.6)$$

where K represent a constant and $\alpha = -0.25$ is the single power law exponent obtained by [15]. Other work based not only on SDSS observations like [15] but also on Λ CDM N -body simulation set $\alpha = -0.9 \pm 0.2$ ([26]). We fix this value to -1.25 and we leave the analysis of the impact of this choice as a future work. Assuming $L_\odot = M_\odot$, we normalize equation 3.6 after setting the support to be the interval of masses that we have available in our catalogue of NIHAO simulations ($10^5 M_\odot < M < 6 \cdot 10^9 M_\odot$) and we sample from this distributions using an inverse scheme. After obtaining the analytic samples we take the first and second Nearest Neighbors (NN) that are within a 10% of the analytic sampled mass as subhalo for our mock halos. We have also set a mass budget

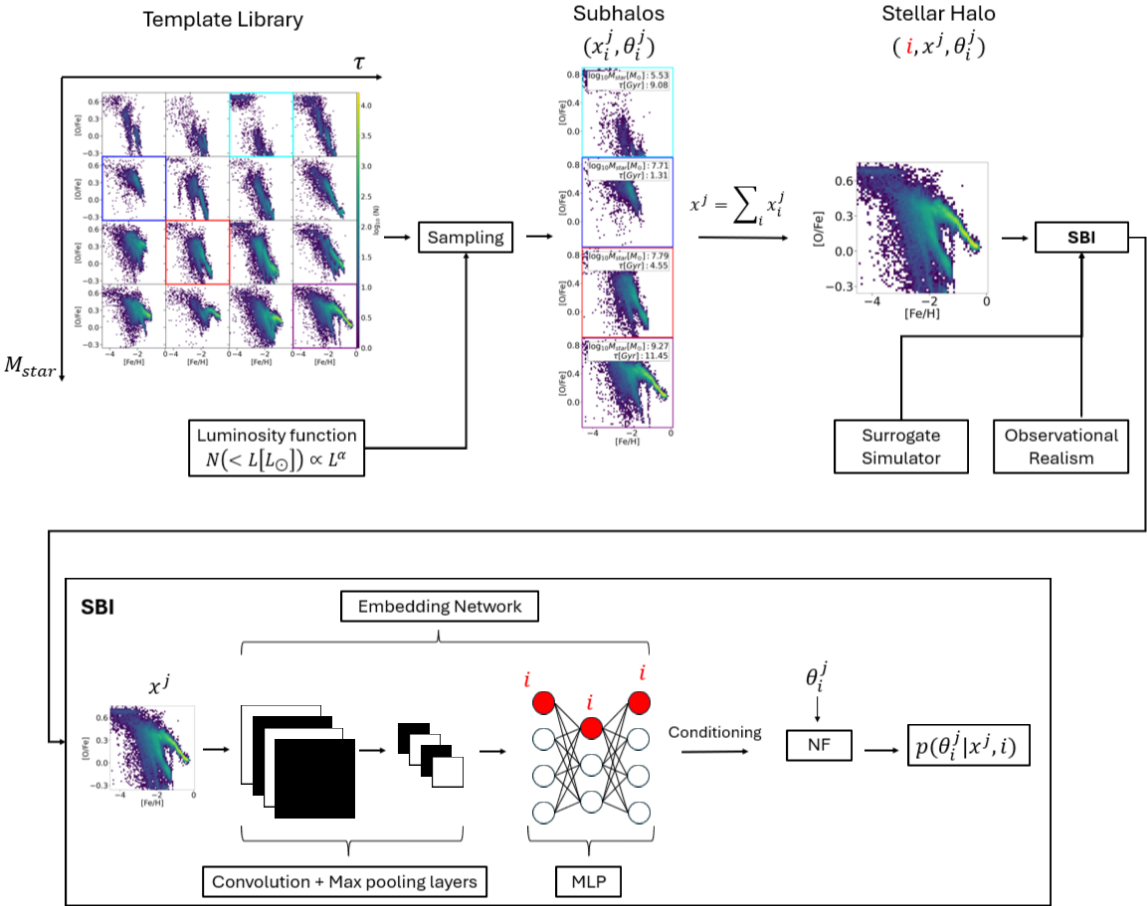


Figure 3.4: CASBI pipeline.

for our mock halo of $M = 1.4 \pm 0.2 \times 10^9 M_{\odot}$ based on [7], and each time a subhalo is sampled we reduce the total mass budget by the mass of the NN that we have used. We decided to put a total mass halo was made in order to avoid to set a fixed number of subhalos that needs to be sampled for each stellar halo. During this iterative procedure we make sure to sample non repeated subhalo within the same mock halo and we avoid repetitions of the same combinations of subhalos between mock subhalos both within training and test set and across these two sets.

In Fig. 3.4 we show the CASBI pipeline. The modularity of the SBI technique is fully integrated, allowing to change all the components of this pipeline. The Template library can be set to be a different any kind of suite of simulated galaxies (e.g. [21]), the sampling scheme can incorporate different luminosity function and stellar halo budget, the NPE and embedding network architecture and hyperparameter can be modified to allow for higher accuracy and posterior coverage thanks to the `optuna` grid search implementation, and surrogate models (Free Form Flow FFF [9], GRUMPY [16]) can be implemented to allow for the sequential version of the NPE.

3.5 Free Form Flow as a surrogate simulator

3.6 Calibration

Chapter 4

Analysis

4.1 NIHAO UHD

Chapter 5

Conclusion

5.1 Future work

5.1.1 GRUMPY

5.1.2 Number halos has a free parameter: hierarchical sbi

5.1.3 True test: GAIA

Bibliography

- [1] The frontier of simulation-based inference. <https://www.pnas.org/doi/10.1073/pnas.1912789117>.
- [2] V. Belokurov, D. Erkal, N. W. Evans, S. E. Koposov, and A. J. Deason. Co-formation of the disc and the stellar halo. *Monthly Notices of the Royal Astronomical Society*, 478(1):611–619, July 2018.
- [3] C. Conroy, A. Bonaca, P. Cargile, B. D. Johnson, N. Caldwell, R. P. Naidu, D. Zaritsky, D. Fabricant, S. Moran, J. Rhee, A. Szentgyorgyi, P. Berlind, M. L. Calkins, S. Kattner, and C. Ly. Mapping the Stellar Halo with the H3 Spectroscopic Survey. *The Astrophysical Journal*, 883(1):107, Sept. 2019.
- [4] X.-Q. Cui, Y.-H. Zhao, Y.-Q. Chu, G.-P. Li, Q. Li, L.-P. Zhang, H.-J. Su, Z.-Q. Yao, Y.-N. Wang, X.-Z. Xing, X.-N. Li, Y.-T. Zhu, G. Wang, B.-Z. Gu, A.-L. Luo, X.-Q. Xu, Z.-C. Zhang, G.-R. Liu, H.-T. Zhang, D.-H. Yang, S.-Y. Cao, H.-Y. Chen, J.-J. Chen, K.-X. Chen, Y. Chen, J.-R. Chu, L. Feng, X.-F. Gong, Y.-H. Hou, H.-Z. Hu, N.-S. Hu, Z.-W. Hu, L. Jia, F.-H. Jiang, X. Jiang, Z.-B. Jiang, G. Jin, A.-H. Li, Y. Li, Y.-P. Li, G.-Q. Liu, Z.-G. Liu, W.-Z. Lu, Y.-D. Mao, L. Men, Y.-J. Qi, Z.-X. Qi, H.-M. Shi, Z.-H. Tang, Q.-S. Tao, D.-Q. Wang, D. Wang, G.-M. Wang, H. Wang, J.-N. Wang, J. Wang, J.-L. Wang, J.-P. Wang, L. Wang, S.-Q. Wang, Y. Wang, Y.-F. Wang, L.-Z. Xu, Y. Xu, S.-H. Yang, Y. Yu, H. Yuan, X.-Y. Yuan, C. Zhai, J. Zhang, Y.-X. Zhang, Y. Zhang, M. Zhao, F. Zhou, G.-H. Zhou, J. Zhu, and S.-C. Zou. The Large Sky Area Multi-Object Fiber Spectroscopic Telescope (LAMOST). *Research in Astronomy and Astrophysics*, 12(9):1197–1242, Sept. 2012.
- [5] E. C. Cunningham, R. E. Sanderson, K. V. Johnston, N. Panithanpaisal, M. K. Ness, A. Wetzel, S. R. Loebman, I. Escala, D. Horta, and C.-A. Faucher-Giguère. Reading the CARDs: The Imprint of Accretion History in the Chemical Abundances of the Milky Way’s Stellar Halo. *The Astrophysical Journal*, 934(2):172, Aug. 2022.
- [6] G. M. De Silva, K. C. Freeman, J. Bland-Hawthorn, S. Martell, E. W. De Boer, M. Asplund, S. Keller, S. Sharma, D. B. Zucker, T. Zwitter, B. Anguiano, C. Bacigalupo, D. Bayliss, M. A. Beavis, M. Bergemann, S. Campbell, R. Cannon, D. Carollo, L. Casagrande, A. R. Casey, G. Da Costa, V. D’Orazi, A. Dotter, L. Duong, A. Heger, M. J. Ireland, P. R. Kafle, J. Kos, J. Lattanzio, G. F. Lewis, J. Lin, K. Lind, U. Munari, D. M. Nataf, S. O’Toole, Q. Parker, W. Reid, K. J. Schlesinger, A. Sheinis, J. D. Simpson, D. Stello, Y.-S. Ting, G. Traven, F. Watson, R. Wittemyer, D. Yong, and M. Žerjal. The GALAH survey: Scientific motivation. *Monthly Notices of the Royal Astronomical Society*, 449(3):2604–2617, May 2015.
- [7] A. J. Deason, V. Belokurov, and J. L. Sanders. The total stellar halo mass of the Milky Way. *Monthly Notices of the Royal Astronomical Society*, 490(3):3426–3439, Dec. 2019.

- [8] A. J. Deason, S. E. Koposov, A. Fattahi, and R. J. J. Grand. Unravelling the mass spectrum of destroyed dwarf galaxies with the metallicity distribution function. *Monthly Notices of the Royal Astronomical Society*, 520(4):6091–6103, Feb. 2023.
- [9] F. Draxler, P. Sorrenson, L. Zimmermann, A. Rousselot, and U. Köthe. Free-form Flows: Make Any Architecture a Normalizing Flow, Apr. 2024.
- [10] C. Durkan, A. Bekasov, I. Murray, and G. Papamakarios. Nflows: Normalizing flows in PyTorch. Zenodo, Nov. 2020.
- [11] A. Helmi, C. Babusiaux, H. H. Koppelman, D. Massari, J. Veljanoski, and A. G. A. Brown. The merger that led to the formation of the Milky Way’s inner stellar halo and thick disk. *Nature*, 563(7729):85–88, Nov. 2018.
- [12] M. Ho, D. J. Bartlett, N. Chartier, C. Cuesta-Lazaro, S. Ding, A. Lapel, P. Lemos, C. C. Lovell, T. L. Makinen, C. Modi, V. Pandya, S. Pandey, L. A. Perez, B. Wandelt, and G. L. Bryan. LtU-ILI: An All-in-One Framework for Implicit Inference in Astrophysics and Cosmology, Feb. 2024.
- [13] D. P. Kingma and P. Dhariwal. Glow: Generative Flow with Invertible 1x1 Convolutions, July 2018.
- [14] E. N. Kirby, G. A. Lanfranchi, J. D. Simon, J. G. Cohen, and P. Guhathakurta. MULTI-ELEMENT ABUNDANCE MEASUREMENTS FROM MEDIUM-RESOLUTION SPECTRA. III. METALLICITY DISTRIBUTIONS OF MILKY WAY DWARF SATELLITE GALAXIES. *The Astrophysical Journal*, 727(2):78, Feb. 2011.
- [15] S. Koposov, V. Belokurov, N. W. Evans, P. C. Hewett, M. J. Irwin, G. Gilmore, D. B. Zucker, H.-W. Rix, M. Fellhauer, E. F. Bell, and E. V. Glushkova. The Luminosity Function of the Milky Way Satellites. *The Astrophysical Journal*, 686(1):279–291, Oct. 2008.
- [16] A. Kravtsov and V. Manwadkar. GRUMPY: A simple framework for realistic forward-modelling of dwarf galaxies. *Monthly Notices of the Royal Astronomical Society*, 514(2):2667–2691, June 2022.
- [17] S. R. Majewski, R. P. Schiavon, P. M. Frinchaboy, C. A. Prieto, R. Barkhouser, D. Bizyaev, B. Blank, S. Brunner, A. Burton, R. Carrera, S. D. Chojnowski, K. Cunha, C. Epstein, G. Fitzgerald, A. E. G. Pérez, F. R. Hearty, C. Henderson, J. A. Holtzman, J. A. Johnson, C. R. Lam, J. E. Lawler, P. Maseman, S. Mészáros, M. Nelson, D. C. Nguyen, D. L. Nidever, M. Pinsonneault, M. Shetrone, S. Smee, V. V. Smith, T. Stolberg, M. F. Skrutskie, E. Walker, J. C. Wilson, G. Zasowski, F. Anders, S. Basu, S. Beland, M. R. Blanton, J. Bovy, J. R. Brownstein, J. Carlberg, W. Chaplin, C. Chiappini, D. J. Eisenstein, Y. Elsworth, D. Feuillet, S. W. Fleming, J. Galbraith-Frew, R. A. García, D. A. García-Hernández, B. A. Gillespie, L. Girardi, J. E. Gunn, S. Hasselquist, M. R. Hayden, S. Hekker, I. Ivans, K. Kinemuchi, M. Klaene, S. Mahadevan, S. Mathur, B. Mosser, D. Muna, J. A. Munn, R. C. Nichol, R. W. O’Connell, J. K. Parejko, A. C. Robin, H. Rocha-Pinto, M. Schultheis, A. M. Serenelli, N. Shane, V. S. Aguirre, J. S. Sobeck, B. Thompson, N. W. Troup, D. H. Weinberg, and O. Zamora. The Apache Point Observatory Galactic Evolution Experiment (APOGEE). *The Astronomical Journal*, 154(3):94, Sept. 2017.

- [18] R. P. Naidu, C. Conroy, A. Bonaca, B. D. Johnson, Y.-S. Ting, N. Caldwell, D. Zaritsky, and P. A. Cargile. Evidence from the H3 Survey That the Stellar Halo Is Entirely Comprised of Substructure. *The Astrophysical Journal*, 901(1):48, Sept. 2020.
- [19] N. Panithanpaisal, R. E. Sanderson, A. Wetzel, E. C. Cunningham, J. Bailin, and C.-A. Faucher-Giguère. The Galaxy Progenitors of Stellar Streams around Milky Way-mass Galaxies in the FIRE Cosmological Simulations. *The Astrophysical Journal*, 920(1):10, Oct. 2021.
- [20] G. Papamakarios. Neural Density Estimation and Likelihood-free Inference, Oct. 2019.
- [21] A. Pillepich, D. Sotillo-Ramos, R. Ramesh, D. Nelson, C. Engler, V. Rodriguez-Gomez, M. Fournier, M. Donnari, V. Springel, and L. Hernquist. Milky Way and Andromeda analogs from the TNG50 simulation, Mar. 2023.
- [22] A. Pontzen, R. Roškar, G. Stinson, and R. Woods. Pynbody: N-Body/SPH analysis for python. *Astrophysics Source Code Library*, page ascl:1305.002, May 2013.
- [23] D. B. Rubin. Bayesianly Justifiable and Relevant Frequency Calculations for the Applied Statistician. *The Annals of Statistics*, 12(4):1151–1172, Dec. 1984.
- [24] M. Steinmetz, T. Zwitter, A. Siebert, F. G. Watson, K. C. Freeman, U. Munari, R. Campbell, M. Williams, G. M. Seabroke, R. F. G. Wyse, Q. A. Parker, O. Bienaymé, S. Roeser, B. K. Gibson, G. Gilmore, E. K. Grebel, A. Helmi, J. F. Navarro, D. Burton, C. J. P. Cass, J. A. Dawe, K. Fiegert, M. Hartley, K. S. Russell, W. Saunders, H. Enke, J. Bailin, J. Binney, J. Bland-Hawthorn, C. Boeche, W. Dehnen, D. J. Eisenstein, N. W. Evans, M. Fiorucci, J. P. Fulbright, O. Gerhard, U. Jauregi, A. Kelz, L. Mijović, I. Minchev, G. Parmentier, J. Peñarrubia, A. C. Quillen, M. A. Read, G. Ruchti, R.-D. Scholz, A. Siviero, M. C. Smith, R. Sordo, L. Veltz, S. Vidrih, R. Von Berlepsch, B. J. Boyle, and E. Schilbach. The Radial Velocity Experiment (RAVE): First Data Release. *The Astronomical Journal*, 132(4):1645–1668, Oct. 2006.
- [25] A. Tejero-Cantero, J. Boelts, M. Deistler, J.-M. Lueckmann, C. Durkan, P. J. Gonçalves, D. S. Greenberg, and J. H. Macke. Sbi: A toolkit for simulation-based inference. *Journal of Open Source Software*, 5(52):2505, Aug. 2020.
- [26] E. J. Tollerud, J. S. Bullock, L. E. Strigari, and B. Willman. Hundreds of Milky Way Satellites? Luminosity Bias in the Satellite Luminosity Function. *The Astrophysical Journal*, 688(1):277–289, Nov. 2008.
- [27] L. Wang, A. A. Dutton, G. S. Stinson, A. V. Macciò, C. Penzo, X. Kang, B. W. Keller, and J. Wadsley. NIHAO project I: Reproducing the inefficiency of galaxy formation across cosmic time with a large sample of cosmological hydrodynamical simulations. *Monthly Notices of the Royal Astronomical Society*, 454(1):83–94, Nov. 2015.
- [28] A. R. Wetzel, P. F. Hopkins, J.-h. Kim, C.-A. Faucher-Giguère, D. Kereš, and E. Quataert. RECONCILING DWARF GALAXIES WITH Λ CDM COSMOLOGY: SIMULATING A REALISTIC POPULATION OF SATELLITES AROUND A MILKY WAY-MASS GALAXY. *The Astrophysical Journal Letters*, 827(2):L23, Aug. 2016.
- [29] B. Yanny, C. Rockosi, H. J. Newberg, G. R. Knapp, J. K. Adelman-McCarthy, B. Alcorn, S. Allam, C. A. Prieto, D. An, K. S. J. Anderson, S. Anderson, C. A. L. Bailer-Jones, S. Bastian, T. C. Beers, E. Bell, V. Belokurov, D. Bizyaev, N. Blythe, J. J. Bochanski, W. N. Boroski, J. Brinchmann, J. Brinkmann, H. Brewington, L. Carey, K. M. Cudworth, M. Evans, N. W.

Evans, E. Gates, B. T. Gänsicke, B. Gillespie, G. Gilmore, A. N. Gomez-Moran, E. K. Grebel, J. Greenwell, J. E. Gunn, C. Jordan, W. Jordan, P. Harding, H. Harris, J. S. Hendry, D. Holder, I. I. Ivans, Ž. Ivezić, S. Jester, J. A. Johnson, S. M. Kent, S. Kleinman, A. Kniazev, J. Krzesinski, R. Kron, N. Kuropatkin, S. Lebedeva, Y. S. Lee, R. F. Leger, S. Lépine, S. Levine, H. Lin, D. C. Long, C. Loomis, R. Lupton, O. Malanushenko, V. Malanushenko, B. Margon, D. Martinez-Delgado, P. McGehee, D. Monet, H. L. Morrison, J. A. Munn, E. H. Neilson, A. Nitta, J. E. Norris, D. Oravetz, R. Owen, N. Padmanabhan, K. Pan, R. S. Peterson, J. R. Pier, J. Platson, P. R. Fiorentin, G. T. Richards, H.-W. Rix, D. J. Schlegel, D. P. Schneider, M. R. Schreiber, A. Schwope, V. Sibley, A. Simmons, S. A. Snedden, J. A. Smith, L. Stark, F. Stauffer, M. Steinmetz, C. Stoughton, M. SubbaRao, A. Szalay, P. Szkody, A. R. Thakar, S. Thirupathi, D. Tucker, A. Uomoto, D. V. Berk, S. Vidrih, Y. Wadadekar, S. Watters, R. Wilhelm, R. F. G. Wyse, J. Yarger, and D. Zucker. SEGUE: A SPECTROSCOPIC SURVEY OF 240,000 STARS WITH $g = 14\text{--}20$. *The Astronomical Journal*, 137(5):4377–4399, May 2009.